Hierarchically Organized Nanoparticle Mesostructure Arrays Formed through Hydrothermal Self-Assembly

Adam Wright,[†] John Gabaldon,[†] D. Bruce Burckel,[‡] Ying-Bing Jiang,[†] Z. Ryan Tian,[‡,§] Jun Liu,[‡,||] C. Jeffrey Brinker,[†,‡] and Hongyou Fan*[,†,‡]

Chemical Synthesis and Nanomaterials Department, Sandia National Laboratories, Albuquerque, New Mexico 87106, and Department of Chemical and Nuclear Engineering, The University of New Mexico/NSF Center of Micro-Engineered Materials, Albuquerque, New Mexico 87131

Received March 10, 2006. Revised Manuscript Received May 3, 2006

We report a new self-assembly pathway that leads to supported and hierarchically organized gold nanoparticle mesostructure arrays on solid substrates such as glass slide, thermal oxide, photopolymer film, and mica. Using the nanoparticle micelle as a building block, hierarchical gold nanoparticle mesostructure arrays were prepared by a hydrothermal nucleation and growth process through self-assembly of nanoparticle micelles and organosilicates under basic conditions. Depending on the substrates used, the shape, order, and orientation of the gold nanoparticle mesostructure during nucleation and growth exhibit distinct features. Transmission electron microscopy and X-ray diffraction results revealed that gold nanoparticles were organized as a face-centered cubic mesostructure with precisely controlled interparticle spacing. Optical characterization using UV−vis spectroscopy shows a characteristic surface plasmon resonance band resulted from the ordered nanoparticle arrays. This method provides new means for colloidal self-assembly and for the fabrication of platforms for surface enhanced Raman scattering-based sensors and electric and optical nanodevices with enhanced thermal, chemical, and mechanical robustness.

Introduction

Synthesis of hierarchically structured materials holds both fundamental and practical importance in optical, electronic, and magnetic devices,[1−6] catalysis and sorption,[7] optical elements,[8] and sensors.[2,3] Prior fabrication efforts include biomimetic,[9−11] self-similar,[12] soft lithography,[13] and rapid printing[14] methods. Recently, more progress has been made in the synthesis of hierarchically ordered nanoparticle/polymer macrostructures through interfacially driven self-assembly of polymers with metal and semiconductor nanoparticles.[15−18] However, it has been recently suggested that it is desirable to synthesize ordered nanoparticle arrays inside inorganic matrixes that provide thermal, chemical, and mechanical robustness needed for enhanced device performance.[3,19,20] Earlier efforts have focused on encapsulation of metal nanoparticles inside sol−gel matrixes through introduction of metal nanoparticles[21] or metal precursors followed by either thermally decomposing or reducing them.[22,23] Recently, mesoporous materials have been used as templates to create hybrid silica materials loaded with metal or semiconducting nanoparticles or nanowires through

* To whom correspondence should be addressed. E-mail: hfan@sandia.gov.
[†] The University of New Mexico/NSF Center of Micro-Engineered Materials
[‡] Sandia National Laboratories
[§] Current address: Department of Chemistry, University of Arkansas, Fayetteville, AR 72701.
[||] Current address: Pacific Northwest National Laboratory, 902 Battelle Boulevard, K2-50, Box 999, Richland, WA 99352.

(1) Black, C. T.; Murray, C. B.; Sandstrom, R. L.; Sun, S. H. *Science* **2000**, *290* (5494), 1131.
(2) Cao, Y. W. C.; Jin, R. C.; Mirkin, C. A. *Science* **2002**, *297* (5586), 1536.
(3) Fan, H. Y.; Yang, K.; Boye, D.; Sigmon, T.; Malloy, K.; Xu, H.; Lopez, G. P.; Brinker, C. *Science* **2004**, *304* (5670), 567−571.
(4) Pileni, M. P. *J. Phys. Chem. B* **2001**, *105* (17), 3358.
(5) Zeng, H.; Li, J.; Liu, J. P.; Wang, Z. L.; Sun, S. H. *Nature* **2002**, *420* (6914), 395.
(6) Xia, Y. N.; Halas, N. J. *MRS Bull.* **2005**, *30* (5), 338.
(7) Dai, S. *Chem.−Eur. J.* **2001**, *7* (4), 763.
(8) Yang, P. D.; Wirnsberger, G.; Huang, H. C.; Cordero, S. R.; McGehee, M. D.; Scott, B.; Deng, T.; Whitesides, G. M.; Chmelka, B. F.; Buratto, S. K.; Stucky, G. D. *Science* **2000**, *287* (5452), 465.
(9) Aizenberg, J.; Weaver, J. C.; Thanawala, M. S.; Sundar, V. C.; Morse, D. E.; Fratzl, P. *Science* **2005**, *309* (5732), 275.
(10) Aksay, I.; Trau, M.; Manne, S.; Honma, I.; Yao, N.; Zhou, L.; Fenter, P.; Eisenberger, P.; Gruner, S. *Science* **1996**, *273* (5277), 892−898.
(11) Mann, S.; Ozin, G. A. *Nature* **1996**, *382* (6589), 313.
(12) Tian, Z. R. R.; Liu, J.; Voigt, J. A.; McKenzie, B.; Xu, H. F. *Angew. Chem., Int. Ed.* **2003**, *42* (4), 414.
(13) Yang, P. D.; Deng, T.; Zhao, D. Y.; Feng, P. Y.; Pine, D.; Chmelka, B. F.; Whitesides, G. M.; Stucky, G. D. *Science* **1998**, *282* (5397), 2244−2246.
(14) Fan, H. Y.; Lu, Y. F.; Stump, A.; Reed, S. T.; Baer, T.; Schunk, R.; Perez-Luna, V.; Lopez, G. P.; Brinker, C. J. *Nature* **2000**, *405* (6782), 56.
(15) Boker, A.; Lin, Y.; Chiapperini, K.; Horowitz, R.; Thompson, M.; Carreon, V.; Xu, T.; Abetz, C.; Skaff, H.; Dinsmore, A. D.; Emrick, T.; Russell, T. P. *Nat. Mater.* **2004**, *3* (5), 302.
(16) Lin, Y.; Boker, A.; He, J. B.; Sill, K.; Xiang, H. Q.; Abetz, C.; Li, X. F.; Wang, J.; Emrick, T.; Long, S.; Wang, Q.; Balazs, A.; Russell, T. P. *Nature* **2005**, *434* (7029), 55.
(17) Lopes, W. A.; Jaeger, H. M. *Nature* **2001**, *414* (6865), 735.
(18) Saunders, A. E.; Shah, P. S.; Sigman, M. B.; Hanrath, T.; Hwang, H. S.; Lim, K. T.; Johnston, K. P.; Korgel, B. A. *Nano Lett.* **2004**, *4* (10), 1943.
(19) Petruska, M. A.; Malko, A. V.; Voyles, P. M.; Klimov, V. I. *Adv. Mater.* **2003**, *15* (7−8), 610−613.
(20) Sundar, V. C.; Eisler, H. J.; Bawendi, M. G. *Adv. Mater.* **2002**, *14* (10), 739.
(21) Fan, H. Y.; Zhou, Y. Q.; Lopez, G. P. *Adv. Mater.* **1997**, *9* (9), 728.
(22) Epifani, M.; Giannini, C.; Tapfer, L.; Vasanelli, L. *J. Am. Ceram. Soc.* **2000**, *83* (10), 2385.
(23) Sarkar, D. K.; Cloutier, F.; El Khakani, M. A. *J. Appl. Phys.* **2005**, *97* (8), 084302.

10.1021/cm060586+ CCC: $33.50
Published on Web 06/02/2006

Scheme 1. Formation of the Water-Soluble Nanoparticle Micelle and Preparation of Hierarchical Nanoparticle Mesostructure Arrays through Hydrothermal Self-Assembly of Water-Soluble Nanoparticle Micelle Building Blocks with Organosilicate[a]

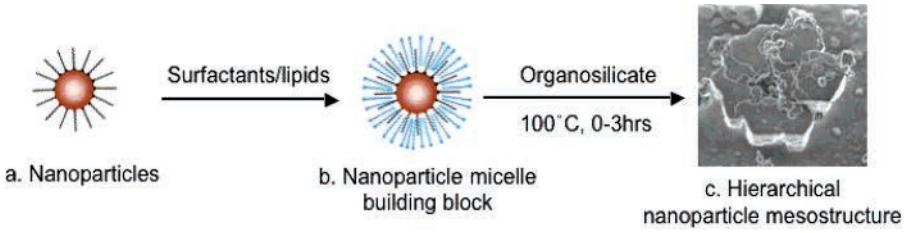

[a] (a) Organic monolayer capped, hydrophobic gold nanoparticles. (b) Nanoparticle micelle building blocks are formed through evaporation-driven transfer of hydrophobic nanoparticles into the interior of surfactant/lipid micelles in an interfacially mediated oil-in-water microemulsion process. (c) Hierarchical nanoparticle mesostructure arrays are formed via a hydrothermal self-assembly process.

infiltration of precursor solutions followed by chemical or electrochemical reduction or direct infiltration of nanoparticles.[24−28] Several disadvantages for the above methods include the following: First, the nanoparticle arrays inside the final materials exhibit poorly defined or less-ordered structure. This is problematic for the fundamental studies of charge transport to get reproducible results. Second, the methods have less control over particle sizes and loading. Third, it is difficult for the above methods to precisely control interparticle spacing that is essential for achieving new physical properties resulting from coupling between neighboring nanoparticles.[5,29,30] Finally, as a result of the unconnected pore channel or dead pore within the porous materials that causes transport problems during infiltration, the resulting materials exhibited vacant areas that were not completely filled with nanoparticles or nanowires.

Here we report a new self-assembly pathway that leads to supported hierarchically ordered gold nanoparticle/organosilicate mesostructure arrays on a glass slide, thermal oxide, a photopolymer film, and mica. Using the nanoparticle micelle as a building block, hierarchically ordered nanoparticle mesostructure arrays were prepared by a hydrothermal nucleation and growth process through self-assembly of nanoparticle micelles and organosilicates under basic conditions. Gold nanoparticles were organized as a face-centered cubic (fcc) mesostructure with precisely controlled interparticle spacing. Depending on the substrates used, the shape, order, and orientation of mesostructures during nucleation and growth exhibit distinct features. The surface plasmon resonance in the visible region resulting from the ordered gold nanoparticle arrays suggests the potential applications for surface enhanced Raman scattering (SERS)-based sensors[2] and electric and optical nanodevices with enhanced thermal, chemical, and mechanical robustness.[18,19]

Experimental Section

All materials were ordered through Aldrich without further purifications.

Sample Preparation. Gold nanoparticles were prepared according to the method reported by Brust et al.[40] using dodecanethiol (1-DT) as a stabilizing ligand. Before precipitation of 1-DT-stablized gold nanoparticles, toluene was first evaporated at 40 °C under vacuum. The resulting waxy black product was then heat treated at 140 °C for 0.5 h. This heat treatment process enables Oswald ripening and allows reorganization in nanoparticle size, leading to much narrower nanoparticle size distribution (∼7%), which is essential to form ordered nanoparticle crystal arrays. Gold nanoparticle micelles were synthesized according to previous work.[3,31−33] A total of 0.1 g of sodium hydroxide was added to 9 mL of gold nanoparticle micelle aqueous solution followed by adding 0.28 g of bis(triethoxylsilyl)ethane (BTEE) in a 20 mL vial. After the solution was stirred for 1 h at room temperature, glass slides or fresh-peeled mica were placed vertically inside these vials. After they were sealed, the vials were placed vertically inside an oven at 100 °C for 0−3 h. The slides were then taken out and rinsed by deionized water and dried.

Characterizations. The X-ray diffraction (XRD) spectra were recorded on a Siemens D500 diffractometer using Ni-filtered Cu Kα radiation with $\lambda = 1.54$ Å in $\theta-2\theta$ ($2\theta = 1-10°$) scan mode using a step size ranging from 0.02° and dwell time of 2 s. Transmission electron microscopy (TEM) images were taken at JEOL 2010 high-resolution microscope equipped with Gatan slow scan charge-coupled device camera and operated at 200 keV. Scanning electron microscopy (SEM) images were taken using Hitachi 5200 microscope.

Results and Discussion

The self-assembly process (shown in Scheme 1) involves two steps: (1) preparation of a building block solution and (2) hydrothermal nucleation and growth of nanoparticle

(24) Fukuoka, A.; Araki, H.; Kimura, J.; Sakamoto, Y.; Higuchi, T.; Sugimoto, N.; Inagaki, S.; Ichikawa, M. *J. Mater. Chem.* **2004**, *14* (4), 752.
(25) Guari, Y.; Theiuleux, C.; Mehdi, A.; Reye, C.; Corriu, R. J. P.; Gomez-Gallardo, S.; Philippot, K.; Chaudret, B.; Dutartre, R. *Chem. Commun.* **2001** (15), 1374.
(26) Guari, Y.; Thieuleux, C.; Mehdi, A.; Reye, C.; Corriu, R. J. P.; Gomez-Gallardo, S.; Philippot, K.; Chaudret, B. *Chem. Mater.* **2003**, *15* (10), 2017.
(27) Brieler, F. J.; Froba, M.; Chen, L. M.; Klar, P. J.; Heimbrodt, W.; von Nidda, H. A. K.; Loidl, A. *Chem.—Eur. J.* **2002**, *8* (1), 185.
(28) Cho, A. T.; Shieh, J. M.; Shieh, J.; Lai, Y. F.; Dai, B. T.; Pan, F. M.; Kuo, H. C.; Lin, Y. C.; Chao, K. J.; Liu, P. H. *Electrochem. Solid State Lett.* **2005**, *8* (6), G143.
(29) Collier, C. P.; Saykally, R. J.; Shiang, J. J.; Henrichs, S. E.; Heath, J. R. *Science* **1997**, *277* (5334), 1978−1981.
(30) Pileni, M. *J. Phys. Chem. B* **2001**, *105*, 3358.
(31) Fan, H. Y.; Leve, E. W.; Scullin, C.; Gabaldon, J.; Tallant, D.; Bunge, S.; Boyle, T.; Wilson, M. C.; Brinker, C. J. *Nano Lett.* **2005**, *5* (4), 645.
(32) (a) Fan, H. Y.; Leve, E.; Gabaldon, J.; Wright, A.; Haddad, R.; Brinker, C. *Adv. Mater.* **2005**, *17*, 2587−2590. (b) Fan, H. Y.; Wright, A.; Gabaldon, J.; Rodriguez, A.; Brinker, C. J.; Jiang Y. B. *Adv. Funct. Mater.* **2006**, *16*, 891−895. (c) Fan, H. Y.; Gabaldon, J.; Brinker, C. J.; Jiang, Y. B. *Chem. Commun.* **2006**, *22*, 2323−2325.
(33) Fan, H. Y.; Chen, Z.; Brinker, C.; Clawson, J.; Alam, T. *J. Am. Chem. Soc.* **2005**, *127*, 13746−13747.

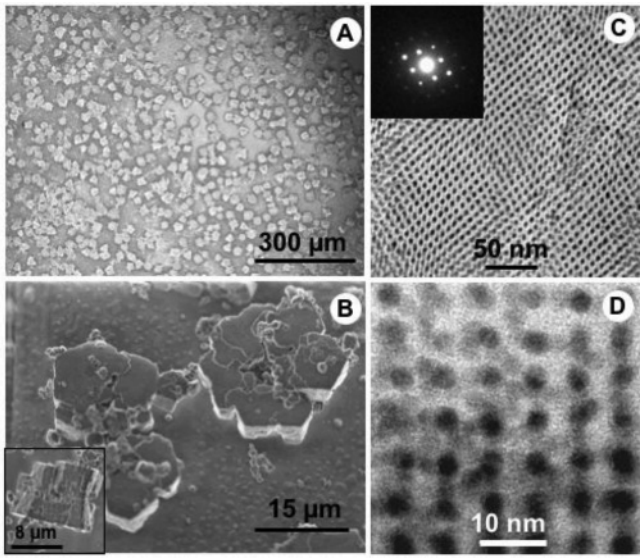

Figure 1. Representative SEM and TEM micrographs of hierarchical nanoparticle mesostructure arrays on glass slides. (A) Sample was prepared on an amorphous glass slide using BTEE as the precursor under basic conditions at 100 °C for 60 min. (B) A magnified SEM image of (A) showing that the hierarchical mesostructure consists of three to five subunits. The inset shows a cross-sectional image of a main unit of the hierarchical mesostructure indicating that the crystal height is ~8 μm. Representative TEM images from [110] orientation (C) and [100] orientation (D). Inset in part C shows the selected area electron diffraction pattern from the image in part C and suggests the three-dimensionally ordered features.

mesostructures. In the first step, the nanoparticle micelles were synthesized through a surfactant encapsulation process[3,31−33] using 1-DT capped gold nanoparticles and cetyltrimethylammonium bromide (CTAB; Scheme 1a). Briefly, a monodisperse, DT-capped gold nanoparticle chloroform solution was added to a CTAB aqueous solution to form an oil-in-water microemulsion under vigorous stirring. The highly volatile chloroform was then removed by heating at ~40 °C for ~10 min. Evaporation of the chloroform induces transfer of DT-capped, hydrophobic gold nanoparticles into the hydrophobic core of surfactant micelles through van der Waals interactions between the interdigitated alkane chains of DT and CTAB, forming water-soluble gold nanoparticle micelles. The second step involves the nucleation and growth of nanoparticle mesostructure arrays in a hydrothermal self-assembly process (Scheme 1b). BTEE was chosen as the precursor for its preferential self-assembly with the micellar interface and formation of well-controlled external topology.[12,34] In a typical synthesis, BTEE and sodium hydroxide are mixed with a nanoparticle micelle aqueous solution in a small vial (see Experimental Section). After 1 h of stirring at room temperature, a substrate such as a microscope slide, thermal oxide coated silicon wafer, or fresh-peeled mica slide was vertically placed inside the small vial. The vials were then sealed and placed inside an oven at 100 °C for crystal growth.

Well-shaped and oriented nanoparticle mesostructure arrays began to grow over several hours. These large nanoparticle mesostructures covered the whole substrate. Figure 1 shows a typical SEM micrograph of large area

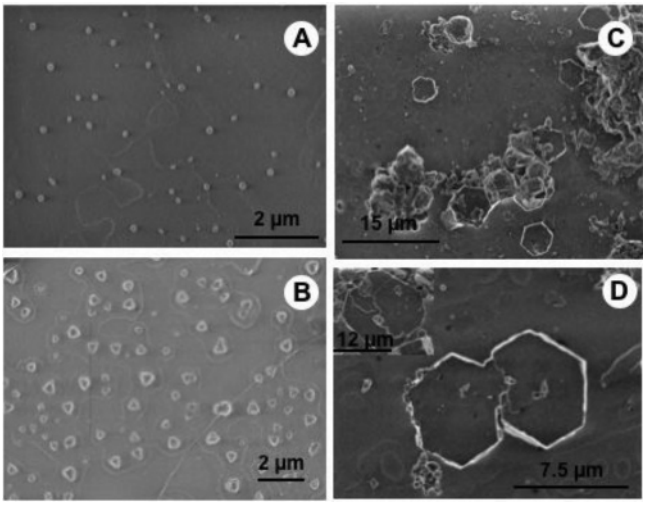

Figure 2. SEM micrographs of samples at different growth times. Results suggest that hierarchical nanoparticle mesostructure arrays are formed through a heterogeneous nucleation and growth process on glass slides. (A) At 10 min, ~0.3 μm particles were observed. (B) At 20 min, crystals with triangular shape were observed. (C, D) At 40 min, a single subunit and some intermediate hierarchical structures have been formed.

arrays of the nanoparticle mesostructures grown on glass slides. They are fairly uniform in shape and size (~15 μm, Figure 1A) with well-defined external topology. The high-resolution SEM image (Figure 1B) shows that each individual main unit exhibits flowerlike hierarchical structure, which consists of three to five subunits with hexagonal shape and size of ~7 μm. A cross-sectional view of the main unit (Figure 1B, inset) shows a height of about 8 μm. The TEM image (Figure 1C,D) and low-angle XRD patterns (Figure 4) reveal that the gold nanoparticles self-assemble as a fcc mesostructure inside the BTEE matrix. Figure 1C,D shows representative TEM images of [110] and [100] orientations of the nanoparticle mesostructure along with its corresponding selected area electron diffraction pattern. The TEM images are consistent with a unit cell of ~10.6 nm and a uniform, minimum interparticle spacing of ~3 nm.

To study the formation mechanism, samples at different growth times were examined by SEM (Figure 2) and XRD patterns (Figure 3). Figure 2A−D shows hierarchical mesostructures after growth for 10, 20, 30, and 40 min. After the initial 10 min, the macroscopic seed sites (size < 0.5 μm) had just begun to form with no recognizable shape. In the XRD (Figure 3A), the appearance of a small hump between 2 and 3° suggests that, at this stage, the nanoparticles have started to self-assemble, exhibiting short range order. After 20 min, the seeds begin to grow into a triangle shape with size between 0.5 and 1 μm. On the XRD patterns, two peaks are observed at low angle corresponding to cubic symmetry. The first sharp peak is attributed to the (111) reflection, and the second broad hump can be assigned to (220) and/or (311). Between 30 and 40 min, hexagon-shaped subunits with a size of 7 μm are developed. They are rather uniform in shape and size. Some of them have merged into hierarchical structures. XRD shows that the fcc mesophase began to form as evidenced by the emergence of (311) and (222) peaks. After 60 min, the hierarchical mesostructures have completely developed, each of which consists of three to five uniformly merged subunits. The XRD (Figure 3A, curve e)

(34) Inagaki, S.; Guan, S.; Ohsuna, T.; Terasaki, O. *Nature* **2002**, *416* (6878), 304−307.

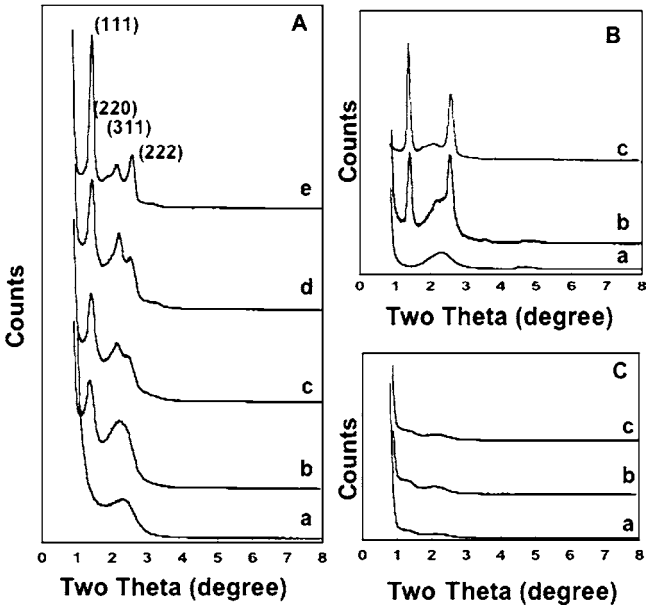

Figure 3. (A) Low angle XRD patterns of hierarchical nanoparticle mesostructure arrays on the glass slide grown (a−e) for 10, 20, 30, 40, and 60 min, respectively. The primary peaks for sample e can be assigned as the (111), (211), (220), and (222) reflections of cubic mesostructure with lattice constant $a = 109.1$ Å. (B) XRD patterns of hierarchical nanoparticle mesostructure arrays on mica grown (a−c) for 10, 30, and 60 min, respectively. (C) XRD patterns of powder samples precipitated in solutions at (a−c) 40, 60, and 120 min, respectively. These patterns show much less order in comparison with those from the hierarchical nanoparticle mesostructures. The samples were prepared using ∼2 nm gold nanoparticles, CTAB surfactant, and sodium hydroxide.

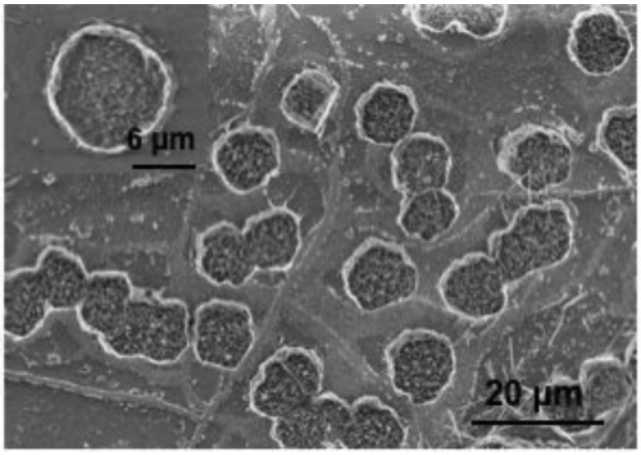

Figure 4. Representative SEM micrograph of hierarchical nanoparticle mesostructure arrays grown on a freshly peeled mica surface using BTEE as the precursor under basic conditions at 100 °C for 60 min. Inset: a magnified SEM image showing an individual mesostructure crystal.

suggests that the fcc gold nanoparticle mesostructure has been fully established by the full appearance of (111), (220), (311), and (222) reflections. The enhanced intensity from the XRD reflections of (111) and (222) during the crystal growth course (after 40 min) suggests an orientated growth with (111) planes parallel to the substrate. This is consistent with the shape changes from triangular to hexagonal shape during the growth phase.

Substrate surface properties strongly influence the nucleation and growth of inorganic materials.[35] In addition to amorphous glasses, other substrates such as mica, thermal oxide coated silicon wafer, and photo-curable polymer films have been successfully used to grow hierarchical nanoparticle mesostructures. In a controlled experiment, fresh-peeled mica was used instead of glass, resulting in a distinct crystal shape. Figure 4 shows a typical SEM image of the large nanoparticle mesostructures formed on a mica surface. As with those grown on glass, they are fairly uniform in shape and size (∼12 μm) but possess circular rather than flowerlike topology and have only one single unit instead of several merged subunits. Another remarkable difference is that the orientated mesostructure began to form at 30 min on mica, earlier than on amorphous glass. This could be due to the fact that mica has a crystalline surface with hexagonal patterns that promotes preferential growth along (111) planes. Similar to the case of amorphous glass, the XRD patterns (Figure 3B, curves b and c) show enhanced reflections of the (111) and (222) planes suggesting the (111) planes of nanoparticle cubic mesostructure are parallel to the substrate. It is noteworthy that prior work in self-assembly of silica and surfactants indicated that only a one-dimensional hexagonal mesophase was formed. It was proposed that surfactants form hemi-rod micelles on the mica surface, leading to a one-dimensional surfactant/silica mesophase.[36] In the current system, nanoparticle micelles are preformed in a homogeneous aqueous solution. Self-assembly with BTEE starts with "hard sphere" nanoparticle micelle building blocks instead of "soft" pure surfactant micelles or liquid crystals. Thus, the cubic mesophase is preferentially formed.

Following growths longer than 40 min, precipitate was observed in the bottom of the vial. To further explore the formation mechanism, we filtered the growth solution and performed XRD studies on the powders. Figure 3C shows the XRD patterns from the precipitated powders after growth for 40, 60, and 120 min. The irregular patterns suggest much less organized nanoparticle/BTEE arrays. This unambiguously establishes that the hierarchical nanoparticle mesostructures are grown from the solution rather than deposited via precipitation. Any gold nanoparticle agglomeration occurring during growth could be expected to have significant impact on the self-assembly process. A UV−vis spectrometer was used to measure the wavelength of the characteristic surface plasmon resonance, providing a measure of the size dispersity of gold nanoparticle micelles in the solution during the growth process: relative to the original DT capped gold nanoparticles, the gold surface plasmon band exhibited no shift, both for as-prepared solutions and after growth for 40, 60, and 120 min (see Supporting Information, Figure S1). This suggests that the gold nanoparticle micelles remain monodisperse during growth and thus that the formation of the mesophase crystals was initiated from nanoparticle micelle building blocks.

The optical properties of the hierarchical nanoparticle mesostructures have been characterized using UV−visible spectroscopy. Figure 5 shows the UV−vis spectra of the hierarchical gold nanoparticle mesostructures on glass and DT-stabilized gold nanoparticles in chloroform. Both samples

(35) Aizenberg, J.; Black, A. J.; Whitesides, G. M. *Nature* **1999**, *398* (6727), 495.

(36) Yang, H.; Kuperman, A.; Coombs, N.; MamicheAfara, S.; Ozin, G. A. *Nature* **1996**, *379* (6567), 703.

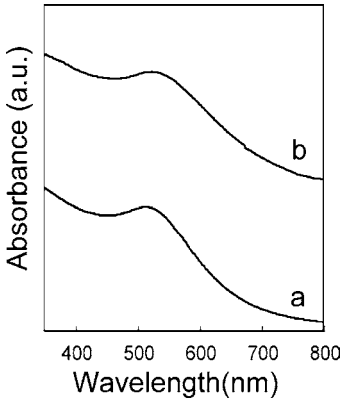

Figure 5. UV−vis spectra of (a) as-prepared DT-capped gold nanoparticles in chloroform and (b) hierarchical nanoparticle mesostructure arrays on the glass slide.

exhibit an absorbance at ~519 nm that corresponds to the gold surface plasmon resonance band. By comparison, we observed no difference in the positions and peak widths of the plasmon resonance band from the hierarchical gold nanoparticle mesostructures and the DT-stabilized gold nanoparticles in chloroform, which implies that gold nanoparticles remain monodisperse inside the BTEE matrix without aggregation and that the hydrothermal self-assembly process does not change the optical property of original DT-stabilized nanoparticles. The results suggest the potential applications of these hierarchical nanoparticle mesostructure arrays for SERS-based sensors and integrated optical and electrical platforms.[2,37] Thermal and mechanical stability is critical for nanoparticle arrays to be applied in practical nanodevices. Heat treatment over time usually broadens the nanoparticle size distribution.[38] We expect that the BTEE framework will provide extensive protection from thermally induced particle agglomeration. After crystal growth at 100 °C for up to 3 h, the gold nanoparticles within the hierarchical mesophase crystals remain monodisperse, as shown by TEM (Figure 1C,D). Results from both TEM and UV−vis spectroscopy imply that the inorganic framework provides enhanced thermal stability, preventing gold nanoparticle aggregation or sintering. Additionally, these hierarchical nanoparticle mesophase crystals show seamless self-assembly features without unit cell distortion or shrinking even after heating to 100 °C for several hours, further confirming the mechanical stability.

Conclusion

We have demonstrated for the first time a new hydrothermal self-assembly process to synthesize hierarchical nanoparticle mesostructures. Results suggest that the formation of such crystals is a nucleation and growth process initiated by self-assembly of nanoparticle micelle building blocks and organo-bridged silane BTEE. The nanoparticles were organized as a cubic mesostructure inside the inorganic framework that allows high-temperature processing. The ease of synthesis of semiconductor and magnetic nanoparticle micelles[31,32] makes it possible to extend this process to synthesize hierarchically ordered semiconductor or magnetic nanoparticle mesostructures. We expect that by using a variety of optical-, electro-, and magnetic-active organo-bridged silanes as framework, we will be able to synthesize multifunctional mesophase crystals with novel collective physical properties.[39] Ultimately, the ordered mesostructure arrays are ideal platforms for fabrication of SERS-based sensors[2] and charge-transfer-based electronic and optical devices.[1,4,6,37]

Acknowledgment. This work was partially supported by the U.S. Department of Energy (DOE) Basic Energy Sciences Program, Sandia National Laboratory's Laboratory Directed R&D program, the Air Force Office of Scientific Research, and Center for Integrated Nanotechnologies (CINT). TEM studies were performed in the Department of Earth and Planetary at the University of New Mexico. We acknowledge the use of the SEM facility supported by the NSF EPSCOR and NNIN grants. Sandia is a multiprogram laboratory operated by Sandia Corporation, a Lockheed Martin Company, for the United States Department of Energy's National Nuclear Security Administration under Contract No. DE-AC04-94AL85000.

Supporting Information Available: UV−vis spectra of as-prepared DT-capped gold nanoparticles in chloroform and as-prepared aqueous solution containing gold nanoparticle micelles, and BTEE after addition of NaOH for 1 h and the solutions after growth for 40 and 60 min (PDF). This material is available free of charge via the Internet at http://pubs.acs.org.

CM060586+

(37) Chen, J.; Wang, W.; Klemic, J.; Reed, M. A.; Axelrod, B. W.; Kaschak, D. M.; Rawlett, A. M.; Price, D. W.; Dirk, S. M.; Tour, J. M.; Grubisha, D. S.; Bennett, D. W. *Mol. Electron. II* **2002**, *960*, 69−99.
(38) Maye, M. M.; Zheng, W. X.; Leibowitz, F. L.; Ly, N. K.; Zhong, C. J. *Langmuir* **2000**, *16* (2), 490.
(39) Hatton, B.; Landskron, K.; Whitnall, W.; Perovic, D.; Ozin, G. A. *Acc. Chem. Res.* **2005**, *38* (4), 305.
(40) Brust, M.; Walker, M.; Bethell, D.; Schiffrin, D. J.; Whyman, R. *Chem. Commun.* **1994**, *7*, 801−802.